Modeling the ionospheric response to the 28 October 2003 solar flare due to coupling with the thermosphere

David J. Pawlowski[1] and Aaron J. Ridley[1]

Received 31 October 2008; revised 29 May 2009; accepted 19 June 2009; published 19 August 2009.

[1] The excess energy deposited into the atmosphere during a solar flare has a substantial effect on the thermosphere and ionosphere. Not only is there a significant perturbation on the dayside, but gravity waves are launched which can propagate to and effect the nightside. The ionospheric signatures of these waves and global disturbances are investigated using the Global Ionosphere-Thermosphere Model during the 28 October 2003 solar flare. Simulations are performed where all external forcings are held constant except for the solar extreme ultraviolet flux in order to quantify the response due only to the flare. The model shows that significant perturbations in N_mF_2 and total electron content can occur on the nightside, and that they can last for more than 15 h after the flare. Both significant enhancements and depletions are shown to be present in the near-midnight sector which are due to dynamical changes in the neutral atmosphere.

Citation: Pawlowski, D. J., and A. J. Ridley (2009), Modeling the ionospheric response to the 28 October 2003 solar flare due to coupling with the thermosphere, *Radio Sci.*, *44*, RS0A23, doi:10.1029/2008RS004081.

1. Introduction

[2] Over the past several decades, an in-depth understanding has been developed of the basic fundamental processes that dominate the climatology of the thermosphere and ionosphere. The dominant source of energy at midlatitudes and low latitudes is the solar extreme ultraviolet (EUV) and soft X-ray radiation, from wavelengths of about 10 through 200 nm. It is these photons that deposit energy in the atmosphere from roughly 120–200 km [*Mayr et al.*, 1985], create the ionosphere and ultimately provide heat to the thermosphere [*Schunk and Nagy*, 2000]. While the motion of the neutrals is generally dominated by the day to night pressure gradient, the presence of a strong intrinsic magnetic field in the Earth causes the electrons and ions to behave differently. At high latitudes, nearly vertical field lines allow charged particles to precipitate and currents to flow from the magnetosphere to ionospheric altitudes, and through Joule heating, contribute to the total energy in the atmosphere. At lower latitudes, the magnetic topology can lead to interesting phenomenon such as the equatorial electrojet [*Forbes*, 1981] and the equatorial anomaly [*Anderson and Roble*, 1981]. During dynamic geomagnetic conditions, penetrating magnetospheric electric fields can cause all of these features to become severely disturbed.

[3] Since the ion density in the upper atmosphere is always small compared to the neutrals, the neutral atmosphere can have a significant effect on the composition and motion of the ionosphere. Changes in the O/N_2 ratio at a given altitude can quickly lead to large changes in the production and loss rates of the important chemical reactions, drastically altering the composition. Also, horizontal neutral flows, which can be as a large as 1000 m/s or more, can induce significant ion flows in midlatitude and low-latitude regions. Since the ions are tied strongly to the field lines, they respond by being pushed higher or lower in altitude, which can substantially alter the height and peak density of the F2 layer.

[4] It is these changes in the ionosphere that have become the subject of more intense research in recent years. Advancement and dependence in spaceborne technology in areas such as navigation, communications, and scientific research are driving a need for an understanding of how the upper atmosphere responds to dynamic inputs to the system. One source of dynamics are sudden changes in the incident solar extreme ultraviolet (EUV) radiation due to solar flares. Several studies have attempted to characterize the ionospheric effects due to flares [e.g., *Afraimovich et al.*, 2001; *Tsurutani et*

[1]Department of Atmospheric, Oceanic, and Space Sciences, University of Michigan, Ann Arbor, Michigan, USA.

0048-6604/09/2008RS004081

al., 2005; *Le et al.*, 2007]. A sudden brightening of the solar flux in the EUV wavelengths causes an increase in the photoelectron production everywhere on the dayside. This can have significant effects on, for example, the propagation of Global Positioning System (GPS) signals, are prone to significant error when there are frequent changes in the total electron content (TEC) between the transmitting spacecraft and the receiver.

[5] A substantial ionospheric response is certainly expected on the dayside during a solar flare, but it is also of interest to investigate how the rest of the ionosphere, including the nightside, may respond to perturbed thermospheric dynamics. *Sutton et al.* [2005], based on data analysis of data from the Champ satellite, show that the thermospheric density can be perturbed by 200–300% at 400 km during severe geomagnetic storms. Also, studies by *Sutton et al.* [2006] and *Liu et al.* [2007] indicate that on the dayside, during strong X-class flares, the neutral density can increase by as much as 60% in just a few hours. Since the ionosphere and thermosphere are highly coupled to each other, it is possible that perturbations in the neutral atmosphere may affect the ionosphere. Through the use of a global coupled ionosphere-thermosphere model, *Pawlowski and Ridley* [2008] show that dayside density enhancements due to a solar flare can launch gravity waves that transport energy efficiently to the nightside. Many hours after the flare, there can be density enhancements on the nightside that are nearly as large as those on the dayside. The present study again makes use of the Global Ionosphere-Thermosphere Model (GITM) [*Ridley et al.*, 2006] to examine how the global perturbations in the neutral atmosphere that result from a flare can affect the ionosphere. Specifically, the ionospheric perturbation that results from traveling neutral atmospheric disturbances during the 28 October 2003 X-class solar flare is presented.

2. Model and Method

[6] GITM solves for the coupled ionosphere-thermosphere system in three-dimensional (3-D) spherical coordinates using a block-based decomposition in the horizontal and an altitude based coordinate in the vertical direction. The resolution in the vertical direction is stretched to approximately 1/3 scale height at the start of the simulation, and fixed in time. The horizontal resolution in GITM is flexible, allowing the user to specify the number of blocks to be used in the latitudinal and longitudinal directions at run time. In this study, a horizontal resolution of 5° latitude by 5° longitude is used. GITM does not assume hydrostatic equilibrium, which means that the vertical momentum equation can be solved self-consistently, allowing for significant vertical flows to develop [*Deng et al.*, 2008a]. *Deng et al.* [2008b] has also investigated the use of non constant gravity in the vertical momentum equation. For a more detailed description of the physics included in GITM, see *Ridley et al.* [2006]. In this study, GITM does not include self-consistent low-latitude electrodynamics.

[7] Like all global models of the atmosphere, GITM must be driven using information about solar flux conditions for a given period of time. During a solar flare, the EUV flux can change drastically in minutes, so ideally, the flux needs to be updated in the model on a similar timescale. In 2001, the Solar Extreme Ultraviolet Experiment (SEE) [*Woods et al.*, 2005] on board the TIMED spacecraft began taking measurements of the EUV irradiance. This data is of great use to modelers since it provides measurements across the spectrum of wavelengths relevant to the upper atmosphere. Still, SEE takes measurements only once every 90 min, which, for the purposes of investigating flares, is too coarse of resolution. However, recently *Chamberlin et al.* [2007] developed the Flare Irradiance Spectral Model (FISM), which makes use of X-ray data from the GOES satellites to interpolate the entire SEE spectrum, improving the temporal resolution to 1-min intervals. For this study, results from FISM have been rebinned to 59 wavelength intervals for use in GITM.

[8] In order to perform a quantitative analysis of the system, GITM is run twice, once using the FISM solar EUV spectrum that included the 28 October flare (the perturbed simulation), and again using a constant spectrum (the unperturbed simulation), where the values were set to the measured flux at the beginning of the day on 28 October. The high-latitude convection patterns are specified by *Weimer* [1996] using constant solar wind values typical of the time period. The solar wind properties were certainly not constant during 28 October; however, the goal of the study is to evaluate the ionospheric response due only to solar forcing. Therefore, the only external source of dynamics to the model in the perturbed simulation is the changing solar flux, and there are no changing external inputs in the unperturbed simulation.

3. Results

[9] A summary of the ionospheric and neutral response to the flare is shown in Figure 1 (top), where the minimum, average, and maximum percent differences are shown beginning at 0 UT on 28 October until 4 UT on 29 October. In addition, the details of the ionospheric response are shown in Figure 2, where contour plots of the vertical TEC percent difference along with the horizontal ion velocity difference vectors (calculated at the H_mF_2 altitude) are plotted every hour beginning at

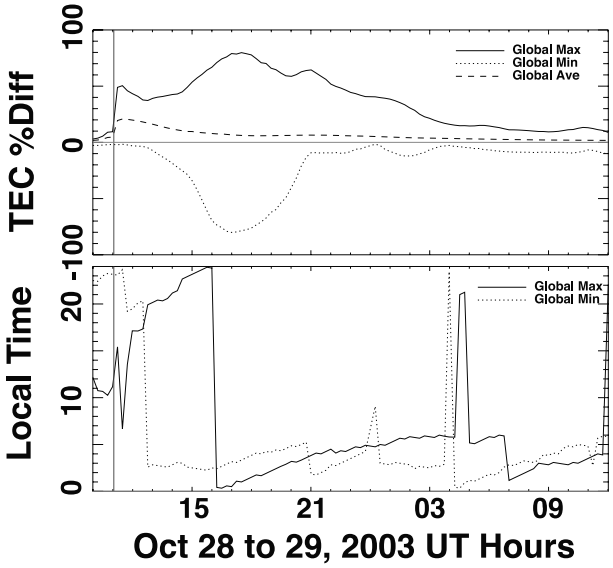

Figure 1. (top) TEC percent difference beginning at 10 UT on 28 October 2003 and ending at 12 UT on 29 October. The solid, dotted, and dashed lines indicate the global maximum, minimum, and average difference between the perturbed and unperturbed runs. The start time of the flare is indicated by the solid gray line just after 11 UT. (bottom) The local time at which the maximum (solid line) and minimum (dotted line) occurs as a function of UT.

13 UT and ending at 22 UT. In both cases, the differences are calculated by the equation:

$$\frac{TEC_{perturbed} - TEC_{unperturbed}}{TEC_{unperturbed}} \times 100,$$

The minimum (maximum) percent difference at any one time is simply the smallest or most negative (largest) difference between the two runs at one cell location, while the average difference is a surface area weighted global mean. The vertical gray line indicates the start time of the flare.

[10] When the flare goes off, there is a clear increase in the globally averaged TEC, which maximizes at about 20%. This is the result of increased photoelectron production on the entire dayside due to the increased EUV flux. Since the average calculation is global, and therefore takes into account the nightside as well as the dayside, this percent difference is lower than it would be if only the dayside average was calculated ($\sim$40%). By 16 UT, this dayside perturbation has subsided (Figure 2), and while the global average difference is still decreasing after 0 UT on 29 October, the difference is minimal.

[11] In addition to the dayside response, there are significant positive and negative perturbations that occur long after the start of the flare. Figure 1 (bottom) shows the local time at which the maximum and minimum perturbations occur. After the flare starts, at 11 UT, the maximum global perturbation is located close to noon. As time elapses, the largest global perturbation propagates toward the nightside at an increasingly slower rate. Conversely, the minimum perturbation remains on the nightside throughout the majority of the time period. These maxima and minima are very localized features that reach their largest magnitudes nearly 6 h after the start of the flare. A more detailed description of the development of these features is shown in Figure 2, which further demonstrates that these enhancements and depletions occur in the nightside ionosphere (i.e., near the blue triangle, which indicates 180° solar zenith angle (SZA)). The largest TEC enhancement develops over the western coast of Australia beginning at 15 UT. By 17 UT, the perturbed simulation reaches a value of 5.9 TECU (where a TECU is 10^{16} electrons m^{-2}) versus an unperturbed value of 3.3 TECU (79.0% difference). At the same time, at strong TEC depletion develops over the western Pacific and moves over the east coast of Australia where the perturbed TEC value reaches 0.56 TECU versus an unperturbed value is 5.6 TECU ($-$80.1% difference).

[12] During this time period, the locations of the perturbations in the TEC are exactly the same as the locations of the perturbations in N_mF_2. Therefore, in order to determine the cause of these ionospheric disturbances, it is useful to consider the dynamics taking place in the F region, as that is where much of the TEC is located.

[13] Since the large changes in the electron density occur on the nightside, local production of electrons is not likely to be the cause of the positive perturbation, especially given that the high-latitude drivers used during the perturbed and unperturbed simulations are identical. Instead, GITM results suggest that these features are a ramification of coupling with the neutral atmosphere. *Pawlowski and Ridley* [2008] shows that during large flares, gravity waves may be launched in the thermosphere that propagate nightward at the local sound speed plus the background wind velocity. While enhanced neutral zonal winds do not have a strong effect on the

Figure 2. TEC percent difference at 10 different times on 28 October 2003 beginning at 13 UT and ending at 22 UT. The vectors show the ion velocity difference between the perturbed and unperturbed runs. Local noon and midnight are indicated by the red circle and blue triangle, respectively.

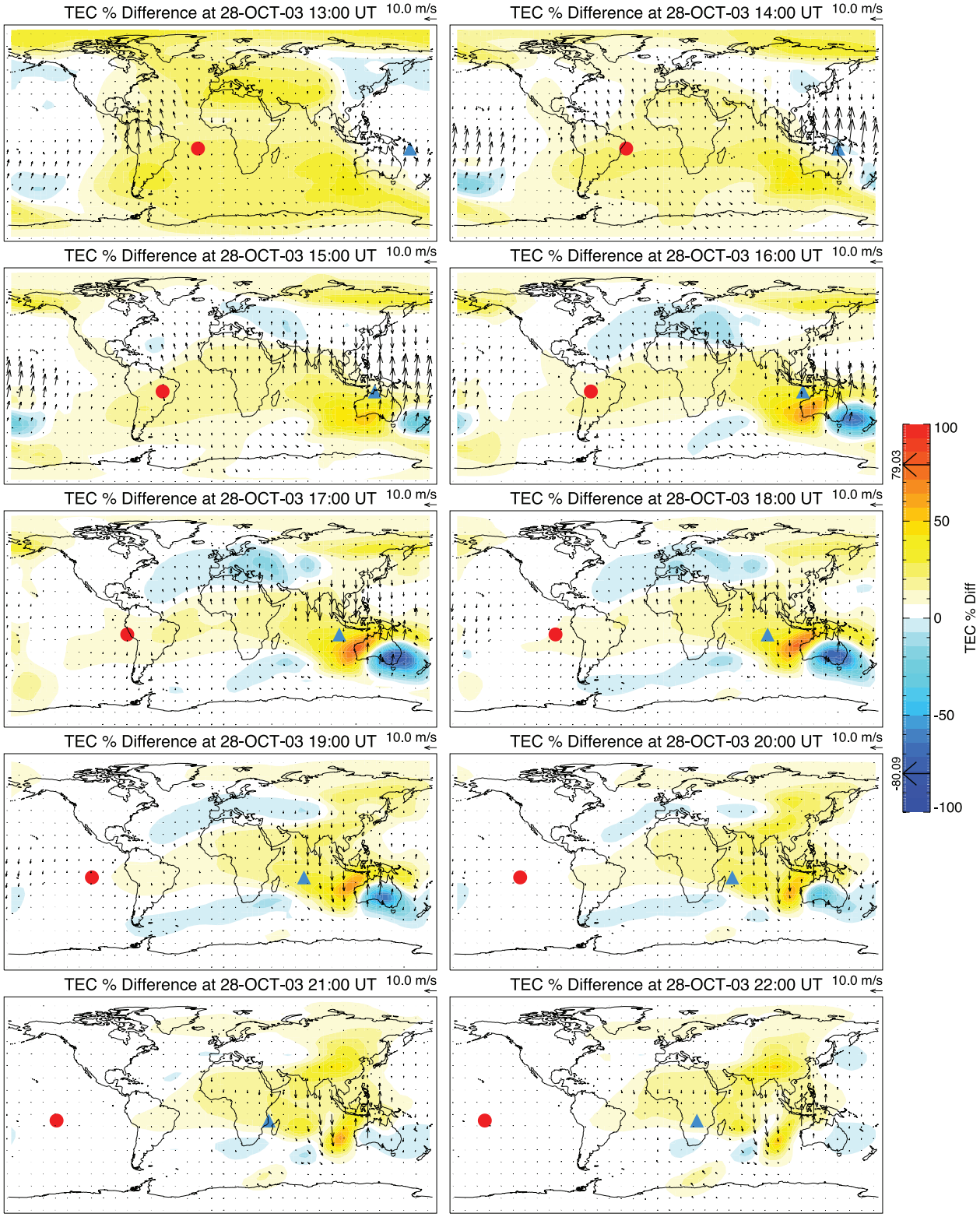
TEC % Difference at 28-OCT-03 13:00 UT
10.0 m/s
TEC % Difference at 28-OCT-03 14:00 UT
10.0 m/s
TEC % Difference at 28-OCT-03 15:00 UT
10.0 m/s
TEC % Difference at 28-OCT-03 16:00 UT
10.0 m/s
TEC % Difference at 28-OCT-03 17:00 UT
10.0 m/s
TEC % Difference at 28-OCT-03 18:00 UT
10.0 m/s
TEC % Difference at 28-OCT-03 19:00 UT
10.0 m/s
TEC % Difference at 28-OCT-03 20:00 UT
10.0 m/s
TEC % Difference at 28-OCT-03 21:00 UT
10.0 m/s
TEC % Difference at 28-OCT-03 22:00 UT
10.0 m/s
100
79.03
50
0
-50
-80.09
-100
TEC % Diff

Figure 2

transport of the charged species because the ions are restricted to motion along the field lines, enhanced neutral meridional winds can result in a larger meridional ion velocity. In this case, beginning at 13 UT, perturbed neutral winds lead to enhanced ion flows in the south pole region and result in a larger tongue of ionization over the south pole in the perturbed simulation, increasing the electron concentration on the nightside. While the ion velocity is relatively unchanged just south of Australia, the stronger ionization tongue is supplying the region with more electrons for the nominal meridional wind, which is setup by the day-to-night pressure gradient as well as the high-latitude convection pattern, to push equatorward. This is shown in Figure 3, in which the electron density at 15 UT (the time at which the nightside positive perturbation is beginning to grow) is plotted at 401 km, which corresponds to the H_mF_2 in the region south of Australia at during this time period. Both the perturbed and the unperturbed simulations are shown. Figure 3 shows that the N_mF_2 south of Australia in the perturbed simulation is approximately 2.4e11 $1/m^3$ whereas the unperturbed N_mF_2 is 1.7e11 $1/m^3$ a difference of 41%. It is important to note that while the absolute difference between the perturbed and unperturbed N_mF_2 in the low latitudes is larger than that south of Australia (approximately 3.8e−11 $1/m^3$), the percent difference is much smaller (14%). After 17 UT, the meridional wind perturbation over the west coast becomes negative as the thermospheric wave reflects back toward the dayside. These enhanced southward winds push the ionosphere down field lines, where the recombination rates are larger due to higher N_2 densities, and the enhancement slowly dies away.

[14] GITM results suggest that the mechanism behind the large negative electron density perturbation that forms over the east Australian coast is also related to dynamics in the ion velocity. The depletion develops at the location where there are enhanced northward ion winds (Figure 2). While this occurs in the near-midnight sector, the location of the perturbation is more than 1 h behind midnight, and therefore the tongue of ionization does not effect the electron density in this region. Without the addition of electrons through the tongue of ionization, the enhanced northward meridional winds push the ionosphere upward in altitude, along field lines. Figure 4 shows the electron density altitude profile for the perturbed simulation (solid lines) and the unperturbed simulation (dashed lines) beginning at 14 UT and ending at 17 UT. In both simulations, the altitude of the peak density is around 350 km at 14 UT. By 15 UT, the H_mF_2 has moved upward, and the density at the top of the model is significantly larger than earlier. As time progresses, the peak density occurs at the top of the model, and the magnitude becomes smaller. This means that there are significant vertical ion flows at all altitudes pushing the electrons out of the model domain. In both simulations, the day-to-night pressure gradient in the thermosphere drives northward neutral winds at this location that result in a nominal upward motion of the ionosphere. However, Figure 4 indicates that the electrons are pushed out of the top boundary faster in the perturbed simulation than in the unperturbed simulation. This is due to the larger northward neutral velocity in the perturbed simulation dragging the ions more quickly up the field lines.

[15] While the upward movement of the ionosphere clearly has an effect on the electron density at a given altitude, the TEC along a field line is not likely to be largely effected because the electrons are only moving to a higher altitude along the same field line. The model indicates a TEC depletion at this time only because the ionosphere has been pushed above the top of the model. In fact, since the ionosphere is being pushed up, slower recombination may actually result in an overall larger TEC magnitude. However, the model results shed light into the importance of neutral coupling on the ionosphere, especially during dynamic time periods. The results indicate that the ability of the enhanced horizontal neutral flows, which develop as a result of a solar flare that began several hours ago on the opposite side of the planet, to lead to significant vertical motion of the ions is important for determining the altitude of the F2 peak, as well as the rest of altitude profile of the ionosphere.

4. Discussion

[16] It is expected that the ionosphere should respond significantly to a solar flare. On the dayside, high EUV fluxes result in higher photoelectron production, and ultimately, a widespread increase in vertical TEC measurements. However, GITM indicates that perturbations in TEC can be more substantial elsewhere in the ionosphere, and that these perturbations can begin many hours after the onset of the solar flare. Traveling thermospheric disturbances, which propagate to the nightside and converge on themselves near midnight, cause substantial compositional and dynamical neutral perturbations. As a result of the changes in the thermosphere, the electron density, and therefore TEC, can be both depleted and enhanced in localized regions on the nightside for more than 15 h after the flare.

[17] The most significant ionospheric perturbations occur in the southern hemisphere around midnight. The largest TEC enhancement, which begins around 15 UT, is due to an enhanced tongue of ionization in the summer hemisphere. It is expected that a similar feature would develop in the northern summer under similar forcing, since, after the flare, the neutral winds are more disturbed in the summer pole than in the winter pole. The location of the depletion that results from the lifting of the of the

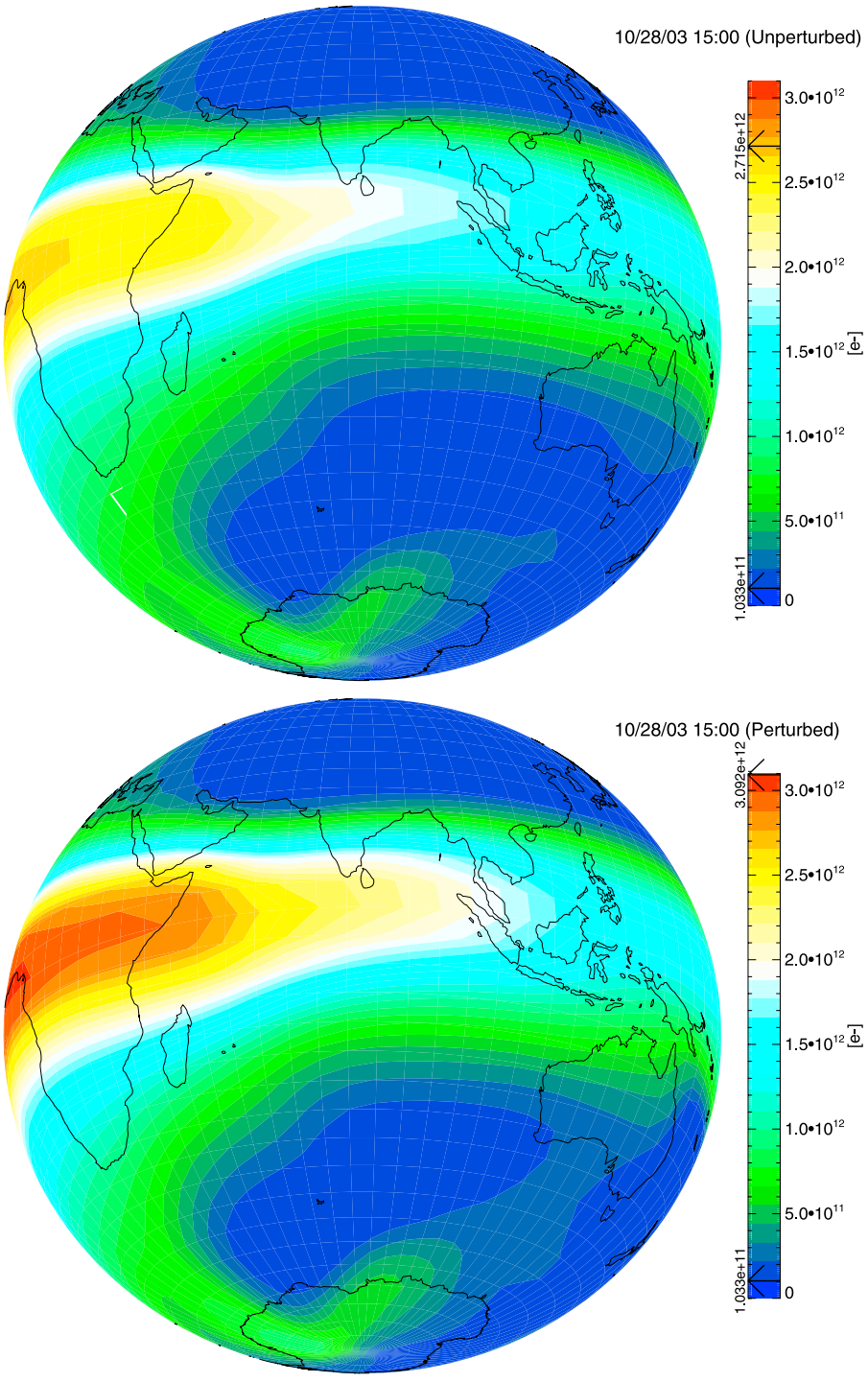

Figure 3. Electron density (m^{-3}) at 15 UT at 401 km for the (top) unperturbed and (bottom) perturbed simulations.

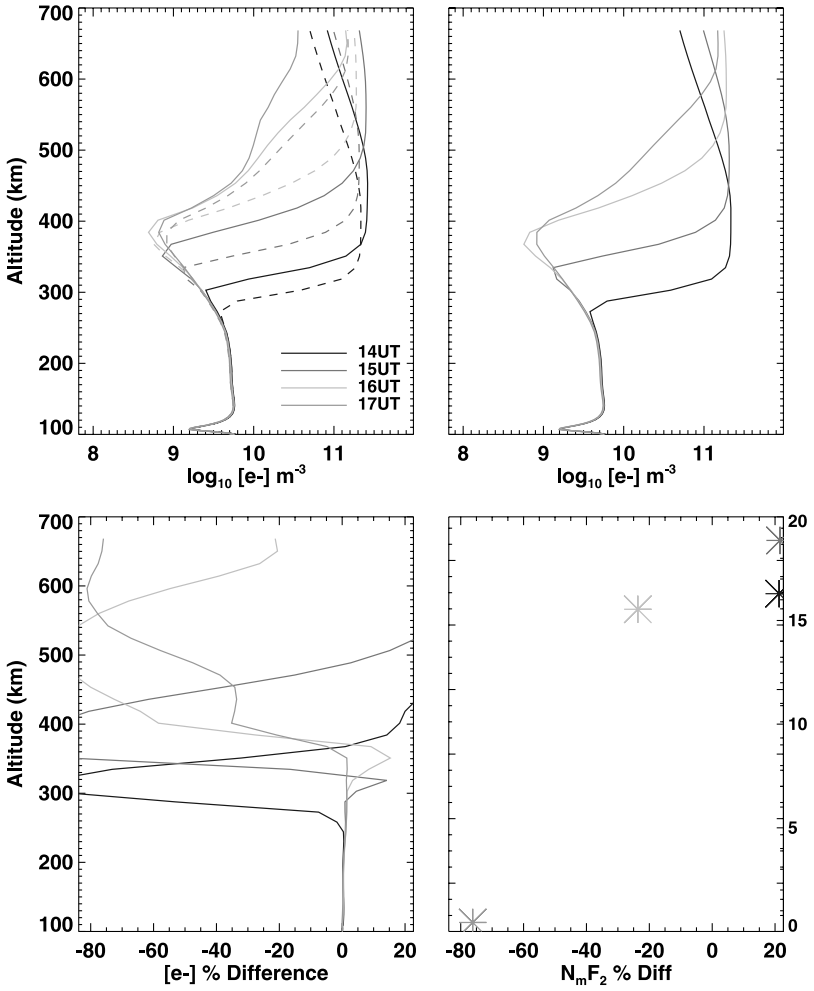

Figure 4. Electron density versus altitude beginning at 14 UT and ending at 17 UT for the unperturbed (dashed lines) and perturbed simulations (solid lines) over the east coast of Australia (152.5°E longitude and 32.5°S latitude).

ionosphere depends on several factors which determine that ability of the neutrals to force the ions, such as where the neutral winds are enhanced as well as the neutral density, and also, the ability of the ions to move vertically (therefore, the inclination of the magnetic field at that location). In this case, the enhanced ion velocities occur where the neutral density and neutral winds are also perturbed, which corresponds to the region of neutral wind convergence on the nightside. Therefore, there is no reason to expect that this feature is limited to the southern hemisphere, but rather, is dependent on the relationship between the location of neutral convergence, the respective density enhancement in that location, and how close that location is to the magnetic equator.

[18] As mentioned, GITM does not include self-consistent low-latitude electrodynamics. The addition of such physics to the model will clearly have an effect on the overall structure of the ionosphere, especially at midlatitudes and low latitudes. In this study, the perturbations that result from the solar dynamics are of interest. The model results indicate that the largest localized perturbations occur on the night-side near Australia. This is far enough south of the magnetic equator such that the addition of low-latitude electrodynamics should have little effect on the magnitude and location of these perturbations. However, given a situation where the convergence of neutral flows on the nightside occurs closer to the magnetic equator, low-latitude electrodynamics are expected to play a more significant role.

[19] These features all have important operational implications due to their localized nature and severity. The perturbations observed in the model are all highly

dependent on both the neutral wind and ion convection patterns and therefore on the current geomagnetic conditions. The ability to predict such features, then, is an extremely difficult task, since it is important to correctly specify the advection of both the ion and neutral species as well as correctly specify the external drivers acting on the system. While global models are well suited for this purpose, more work must be done to further understand the important physics taking place. It is important to continue to validate models against in situ data taken in both the thermosphere and ionosphere so that further understanding about the global nature of the response of both the neutral and ionized atmosphere to solar flare events can be developed. In future work, a data analysis study will be performed to investigate how the observed magnitudes of ionospheric perturbations resulting from a flare compare to the model results.

[20] **Acknowledgments.** FISM data were obtained from the LISIRD data archive at http://lasp.colorado.edu/LISIRD/fism.htm. The authors would like to thank Phil Chamberlin, the PI on the FISM project, and Tom Woods, the PI for the SEE mission, for making this data available. This study was supported in part by NSF grants 0539053 and ATM0639336.

References

Afraimovich, E. L., A. T. Altynsev, V. V. Grechnev, and L. A. Leonovich (2001), Ionospheric effects of the solar flares as deduced from global GPS network data, *Adv. Space Res.*, *27*, 1333–1338.

Anderson, D. N., and R. G. Roble (1981), Neutral wind effects on the equatorial F-region ionosphere, *J. Atmos. Terr. Phys.*, *43*, 835–843.

Chamberlin, P. C., T. N. Woods, and F. G. Eparvier (2007), Flare Irradiance Spectral Model (FISM): Daily component algorithms and results, *Space Weather*, *5*, S07005, doi:10.1029/2007SW000316.

Deng, Y., A. D. Richmond, and A. J. Ridley (2008a), Assessment of the non-hydrostatic effect on the upper atmosphere using a general circulation model (GCM), *Geophys. Res. Lett.*, *35*, L01104, doi:10.1029/2007GL032182.

Deng, Y., A. J. Ridley, and W. Wang (2008b), Effect of the altitudinal variation of the gravitational acceleration on the thermosphere simulation, *J. Geophys. Res.*, *113*, A09302, doi:10.1029/2008JA013081.

Forbes, J. M. (1981), The equatorial electrojet, *Rev. Geophys.*, *19*, 469–504.

Le, H., L. Liu, B. Chen, J. Lei, X. Yue, and W. Wan (2007), Modeling the responses of the middle latitude ionosphere to solar flares, *J. Atmos. Sol. Terr. Phys.*, *69*, 1587–1598, doi:10.1016/j.jastp.2007.06.005.

Liu, H., H. Lühr, S. Watanabe, W. Köhler, and C. Manoj (2007), Contrasting behavior of the thermosphere and ionosphere in response to the 28 October 2003 solar flare, *J. Geophys. Res.*, *112*, A07305, doi:10.1029/2007JA012313.

Mayr, H. G., et al. (1985), On the structure and dynamics of the thermosphere, *Adv. Space Res.*, *5*, 283–288, doi:10.1016/0273-1177(85)90151-6.

Pawlowski, D. J., and A. J. Ridley (2008), Modeling the thermospheric response to solar flares, *J. Geophys. Res.*, *113*, A10309, doi:10.1029/2008JA013182.

Ridley, A. J., Y. Deng, and G. Toth (2006), The global ionosphere-thermosphere model, *J. Atmos. Sol. Terr. Phys.*, *68*, 839.

Schunk, R. W., and A. F. Nagy (2000), *Ionospheres*, Cambridge Univ. Press, New York.

Sutton, E. K., J. M. Forbes, and R. S. Nerem (2005), Global thermospheric neutral density and wind response to the severe 2003 geomagnetic storms from CHAMP accelerometer data, *J. Geophys. Res.*, *110*, A09S40, doi:10.1029/2004JA010985.

Sutton, E. K., J. M. Forbes, R. S. Nerem, and T. N. Woods (2006), Neutral density response to the solar flares of October and November, 2003, *Geophys. Res. Lett.*, *33*, L22101, doi:10.1029/2006GL027737.

Tsurutani, B. T., et al. (2005), The October 28, 2003 extreme EUV solar flare and resultant extreme ionospheric effects: Comparison to other Halloween events and the Bastille Day event, *Geophys. Res. Lett.*, *32*, L03S09, doi:10.1029/2004GL021475.

Weimer, D. R. (1996), A flexible, IMF dependent model of high-latitude electric potential having "space weather" applications, *Geophys. Res. Lett.*, *23*, 2549.

Woods, T. N., F. G. Eparvier, S. M. Bailey, P. C. Chamberlin, J. Lean, G. J. Rottman, S. C. Solomon, W. K. Tobiska, and D. L. Woodraska (2005), Solar EUV Experiment (SEE): Mission overview and first results, *J. Geophys. Res.*, *110*, A01312, doi:10.1029/2004JA010765.

D. J. Pawlowski and A. J. Ridley, Department of Atmospheric, Oceanic, and Space Sciences, University of Michigan, Ann Arbor, MI 48109-2143, USA. (dpawlows@umich.edu)